

# Quantification of reflected wave magnitude and transit time using a multi-Rayleigh flow waveform model: A simplified approach to arterial wave separation analysis

Rahul Manoj<sup>a,\*</sup>, P.M. Nabeel<sup>b</sup>, V. Raj Kiran<sup>b</sup>, Mohanasankar Sivaprakasam<sup>a,b</sup>, Jayaraj Joseph<sup>a</sup>

<sup>a</sup> Department of Electrical Engineering, Indian Institute of Technology Madras, Chennai, India

<sup>b</sup> Healthcare Technology Innovation Centre, Indian Institute of Technology Madras, Chennai, India

## ARTICLE INFO

### Keywords:

Arterial pulse wave reflection

Reflection wave transit time

Reflection magnitude

Flow modelling

Carotid artery

Wave separation analysis

## ABSTRACT

Quantification of wave reflection necessitates the simultaneous measurement of pressure and flow waveforms from the same arterial site, enabling wave separation analysis (WSA). A simplified approach to WSA, which involves modelling the flow waveform, offers a methodological advantage over the conventional method. Nevertheless, the current methods of pressure-only WSA is constrained to the aortic site. In this study, we propose a method to model the carotid artery flow rate waveform using multi-Rayleigh functions ( $Q_{m-RAY}(t)$ ) for WSA ( $WSA_{m-RAY}$ ). The carotid artery is associated with central and cerebral haemodynamics and has an anatomical advantage for easier accessibility of non-invasive measurements, unlike the aorta. The accuracy of the  $Q_{m-RAY}(t)$  was assessed against the actual carotid flow rate waveform ( $Q_{REF}(t)$ ), and the performance of the  $WSA_{m-RAY}$  was evaluated against the  $Q_{REF}(t)$  based WSA ( $WSA_{REF}$ ) on 4374 virtual (healthy) subjects. The  $Q_{m-RAY}(t)$  has captured the time instants of characteristic peaks in the flow profile of the common carotid artery with an RMSE < 8.26 ms (<1 % of average heart rate). A strong and statistically significant correlation ( $r = 0.99$ ,  $p < 0.001$ ) was observed for both  $\Delta P_F$  and  $\Delta P_B$  when compared between  $WSA_{REF}$  and  $WSA_{m-RAY}$ . The reflection quantification indices obtained from  $WSA_{REF}$  and  $WSA_{m-RAY}$  yielded strong and statistically significant correlation ( $r > 0.78$ ,  $p < 0.001$ ). The  $WSA_{m-RAY}$  demonstrated the capability to ease the carotid WSA by modelling the flow rate waveform and thereby expanding the possibilities for vascular screenings and diagnostics that rely on single pulse waveform measurements.

## 1. Introduction

During a cardiac cycle, the contraction of the left ventricle produces an impulse that travels with a finite speed along the arteries, creating a forward-running wave. However, the arterial system doesn't completely absorb this wave, resulting in multiple backward-running waves returning to the left ventricle [1] and to the central arteries. The source of reflections in the vasculature is the mismatch of impedance (properties of the pulse wave propagating medium) as seen by the forward wave. These reflections are partially caused by changes in both structural properties (such as diameter tapering and vessel branching) and material properties (like stiffness and stiffness gradient) as the waves move from elastic central to muscular peripheral arteries. At any arterial site, the measured pressure and flow waveforms are a superposition of a forward-running wave, multiple reflections, and re-reflections of the

forward-running wave. The reflection of pressure waves causes pressure augmentation (widening the pulse pressure) in the blood pressure of central arteries, altering the hemostasis at the microcirculation and leading to end-organ damage [2]. Conversely, the early onset of backward waves during the systolic phase increases cardiac afterload [3] and reduces ventricular pump efficiency [4]. The backward travelling pressure wave and pressure augmentation are associated with increased left ventricle mass [5], risk of heart failure [6] and mortality [7]. The transit time between forward and backward waves is of potential clinical value and helps understand the physiologic changes in central blood pressure waveform and a critical aspect of pulsatile ventricular load [8].

In clinical research, the augmentation index (AIx) has gained significant attention as a method for quantifying reflections from central blood pressure waveforms. However, several factors such as the height of the individual, accurate identification of shoulder point or inflection

\* Corresponding author.

E-mail address: [rahulmanojkty@gmail.com](mailto:rahulmanojkty@gmail.com) (R. Manoj).

<https://doi.org/10.1016/j.bspc.2024.106129>

Received 22 June 2023; Received in revised form 8 January 2024; Accepted 18 February 2024

Available online 29 February 2024

1746-8094/© 2024 Elsevier Ltd. All rights reserved.

point, compounding effect of heart rate and arterial stiffness gradient challenge the reliability of AIx and have a debatable role in quantifying reflections [9]. A comparison to wave separation analysis (WSA) has highlighted the limitations of AIx in accurately quantifying reflections [10]. The WSA is widely considered the more reliable “gold standard” for assessing reflection magnitude and timing [1]. For precise WSA, simultaneous measurement of arterial pressure and blood flow waveform are required, preferably from a single arterial site. The WSA decomposes the pressure and flow rate waveform into its respective forward and backward components. Implementation of WSA can be performed through impedance analysis in the frequency domain [11] or through successive wavefront analysis in the time domain [12]. Simultaneous and synchronized acquisition of pressure and flow waveform from the same arterial site (aortic) often imposes a practical challenge for non-invasive measurements. The non-invasive measurement of aortic pressure waveform is indirectly obtained as calibrated and scaled version of the carotid artery or radial artery tonometry waveforms via transfer functions [13]. The aortic flow rate waveforms are obtained from the flow velocity waveforms using Doppler echocardiography or magnetic resonance imaging (MRI) of the left ventricle outflow tract (LVOT) combined with the vessel’s cross-sectional area. However, measuring aortic flow requires trained personnel and access to cardiac echocardiography or MRI equipment and, therefore, may not always be feasible for measuring the aortic flow.

Subsequently, simplified approaches to WSA have been proposed based on approximations to flow waveform [14–20]. The approximations to the flow morphology were first proposed using a triangle waveform, modelled based on the occurrence of time instant of peak flow and ejection period of the heart [14]. Recent studies using flow modelling approaches based on lognormal approximation [17], Windkessel-based [16,21] and personalized modelling [18] of aortic flow have illustrated the alternatives to measuring the aortic flow. However, extensive population studies confirmed that more physiologic modelling of flow waveform is required for accurate WSA, and the discrepancies associated with various methods are described elsewhere [15,18]. Although the WSA is applicable to any pressure and flow waveform measured from the same arterial site, the applicability and validation of simplified WSA were limited to aortic flow waveforms in the literature.

This article proposes a method to model the carotid artery flow rate waveform that is more physiologic and personalized to each participant. The WSA performed at the carotid artery is of interest due to its association with central arteries, closely representing aortic conditions and for its practical advantages in easier accessibility for non-invasive measurements. Additionally, the forward and backward waves from the carotid artery are associated with the rate of cognitive decline and the pathophysiology of cerebral tissues [22]. The carotid artery is the gateway to cerebral circulation, and being a direct branch of the aorta makes it a surrogate for both cerebral and central haemodynamics. Recent studies [23–27] indicate a potential association between the arterial characteristics of the upper body and the development of cerebral microvascular diseases. The vascular pathophysiology underlying these conditions is linked to the strength of pulse waves generated in the craniospinal cavity by the vasculature of the upper body [28]. It’s important to note that the flow waveforms in the upper body differ inherently from those observed in the ascending aorta or lower body arteries. Recent investigations employing WSA on carotid pressure and flow waveforms have demonstrated the ability to predict the onset of mild cognitive impairment more than a decade before clinical diagnosis [22]. The carotid wave intensity analysis (WIA) performed after the separation of forward–backward waves is also gaining interest [29,30] paving way for various perturbation studies in healthy and diseased populations. The recent interest in the carotid artery is mainly attributed to the accessibility to non-invasive sensing technologies and larger number of measurements performed at the carotid artery in comparison to the aorta. This article proposes a multi-Rayleigh flow rate modelling

for carotid flow modelling for WSA and validates the method against the reference flow based WSA. The performance is evaluated in terms of the reflection quantification indices across a broad age group (25 years to 75 years) of 4374 virtual (healthy) subjects.

## 2. Materials & methods

This section is further divided into i) theory, ii) computation and iii) statistical analysis. The former sub-section details the underlying theoretical concepts of wave separation analysis and construction of the multi-Rayleigh flow rate waveform. The latter two sub-sections describe the data preparation, processing and essential statistical analyses performed to validate the proposed method against the reference method. Fig. 1 provides an overview of the proposed carotid WSA using the multi-Rayleigh flow rate model.

### 2.1. Theory

#### 2.1.1. Wave separation analysis and quantification of reflection

The pressure waveform at any arterial site is a superposition of a forward ( $P_F(t)$ ) and backward wave ( $P_B(t)$ ). The separation of forward–backward waves is based on combining the water-hammer theory with the electrical transmission line model [11], as described in (1) and (2).

$$P_F(t) = \frac{1}{2}(P(t) + Q(t) \times Z_C) \quad (1)$$

and

$$P_B(t) = \frac{1}{2}(P(t) - Q(t) \times Z_C) \quad (2)$$

Where  $Z_C$  is the magnitude of the characteristic impedance of the blood vessel from which the  $P(t)$  and  $Q(t)$  are obtained. The  $Z_C$  is estimated either in the time domain [12] from the measure of pulse wave velocity ( $C$ ), the density of blood and the cross-sectional area ( $A$ ) of the blood vessel ( $Z_C = \rho C/A$ ) or in the frequency domain [11] as the average of 4 to 10 harmonics of input impedance  $Z_0$  ( $Z_0 = |P(j\omega)/Q(j\omega)|$ ). The  $Q(t)$  in the expression (1) and (2) is either measured or modelled flow rate waveform. The actual value of  $Q(t)$  will be referred to hereafter as  $Q_{REF}(t)$ , and the wave separation analysis (WSA) obtained using  $Q_{REF}(t)$  as  $WSA_{REF}$ .

The pulse pressure  $\Delta P_F$  and  $\Delta P_B$  are calculated from the amplitudes of  $P_F(t)$  and  $P_B(t)$ , respectively. The ratio of  $\Delta P_B$  to  $\Delta P_F$  is termed as reflection magnitude (RM), and the ratio of  $\Delta P_B$  to the sum of  $\Delta P_F$  and  $\Delta P_B$  is defined as the reflection index (RI), often expressed as a percentage. The reflection wave transit time (RWTT) is the time taken by the  $P_B(t)$  to travel from the reflection site back to the measurement site. There are several methods to calculate RWTT; in this study, it is calculated from the time delay between zero-crossing of mean subtracted  $P_F(t)$  and  $P_B(t)$  [9].

#### 2.1.2. Construction of Multi-Rayleigh flow rate model

A healthy human’s carotid artery flow rate waveform is predominantly antegrade and triphasic, exhibiting characteristic peaks in early systole, late systole and early diastole [31]. An illustration of the characteristic features of the carotid flow rate waveform is depicted in the Supplementary Fig. (SF 1). The relative amplitudes of early systolic and late systolic peaks strongly associate with corresponding carotid pressure augmentation [27]. Therefore, the flow rate waveform modelling is based on this underlying association of pulse contours of  $Q_{REF}(t)$  with  $P(t)$ , which is explored using the second derivative waveforms of  $P(t)$ . Fig. 2 illustrates the construction of multi-Rayleigh flow rate waveform from pulse contours of  $P(t)$ .

The Rayleigh curves are a skewed form of a Gaussian curve which is characterized by a steeper upstroke and a gradual downstroke, a feature

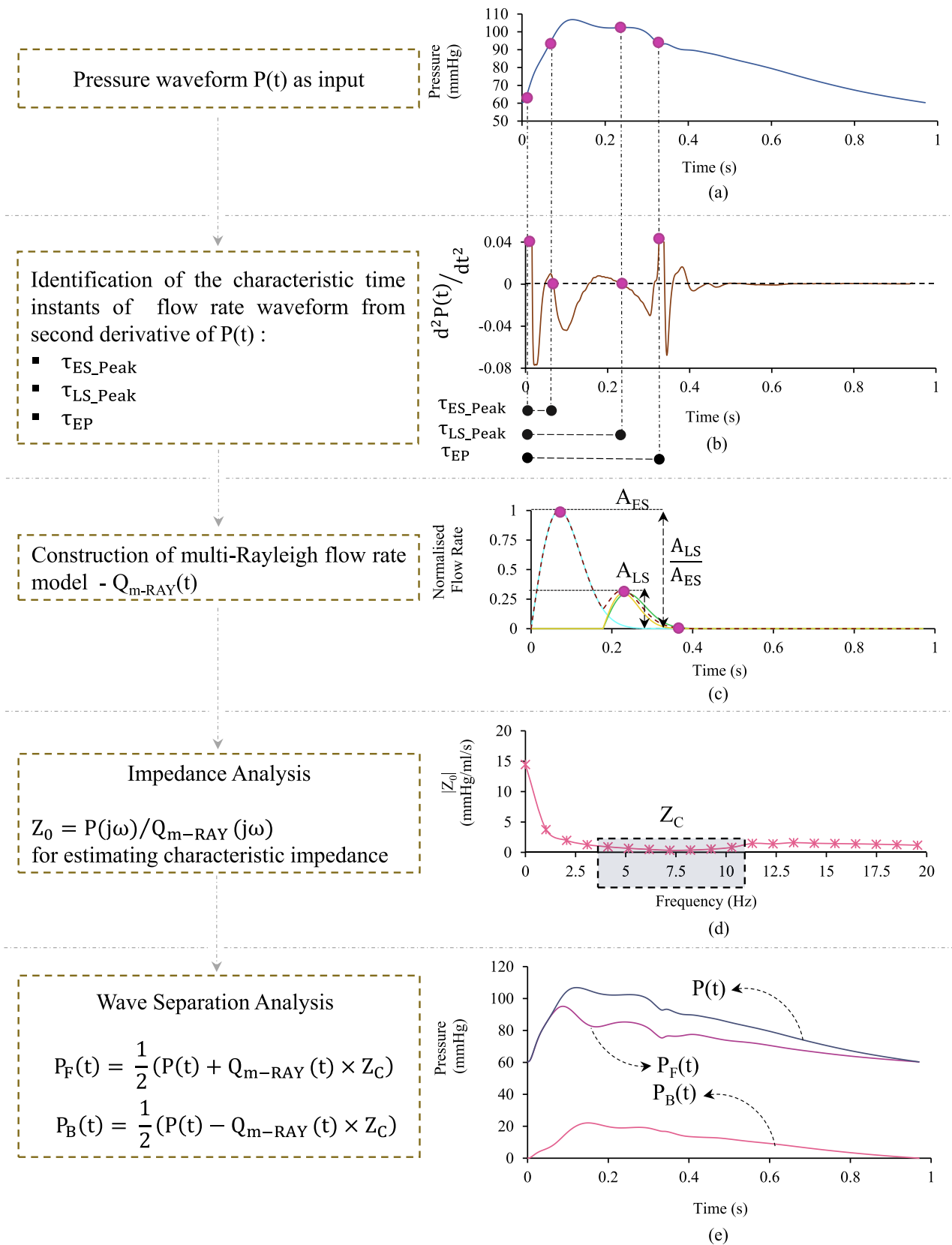
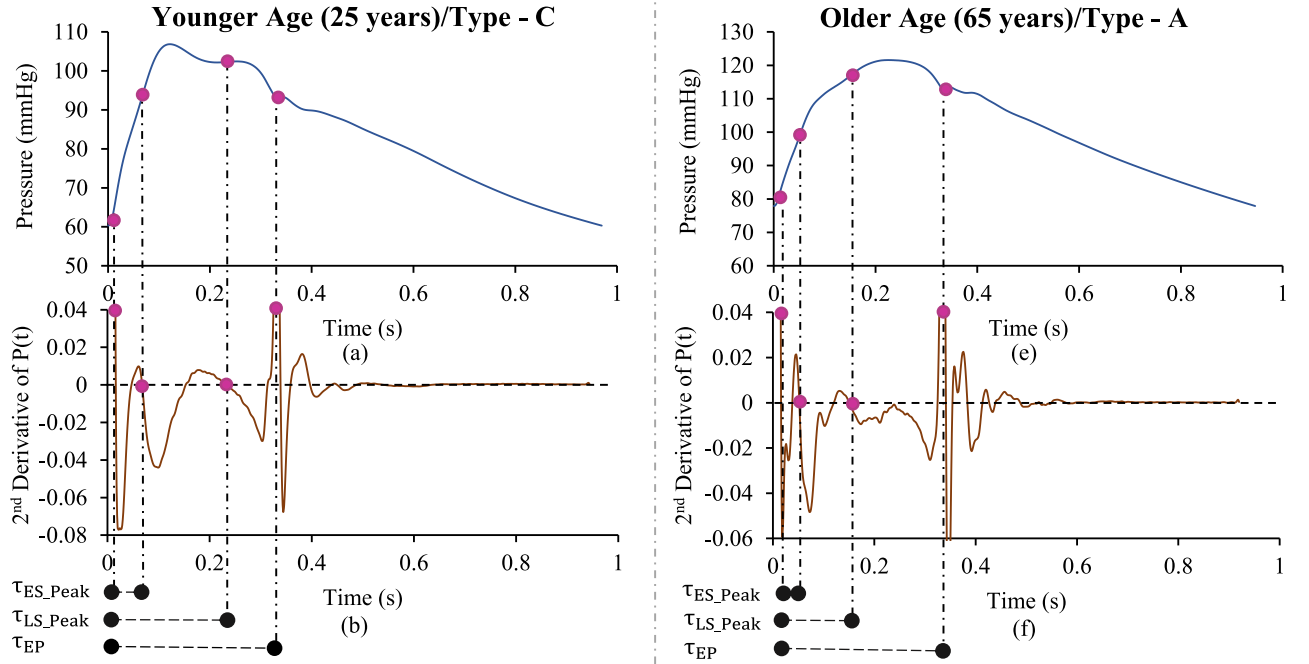
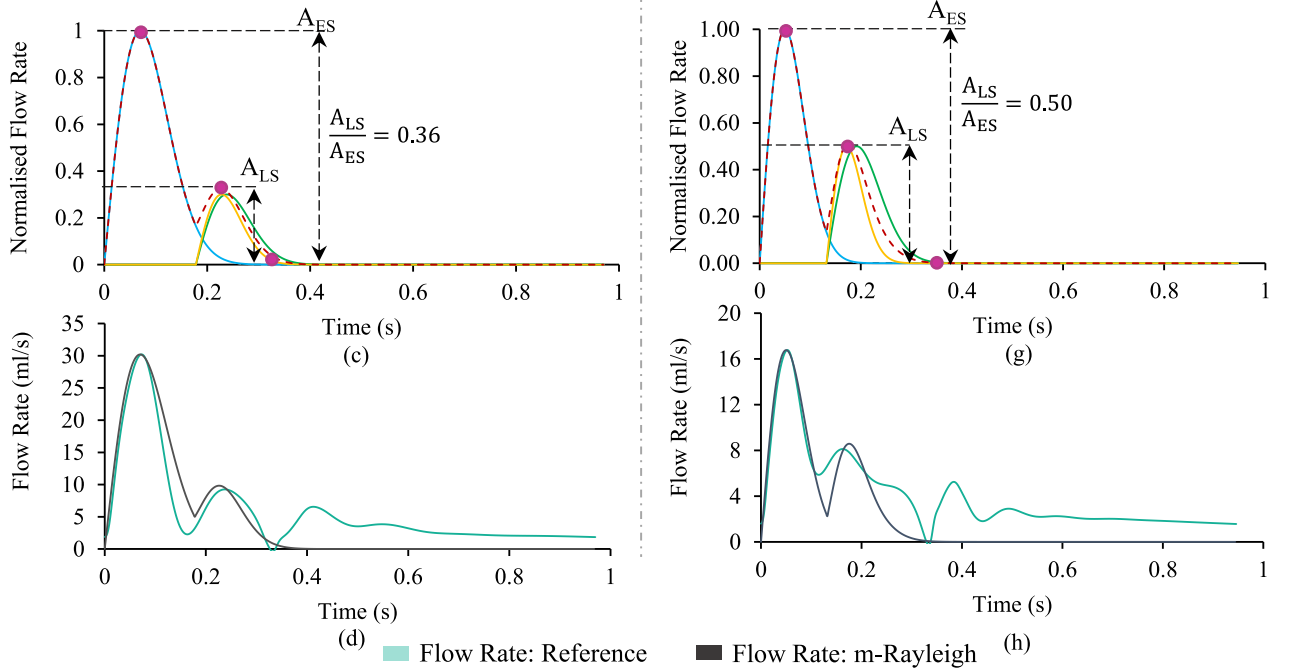


Fig. 1. Overall description and algorithm of the proposed multi-Rayleigh flow rate model for carotid WSA. (a) Carotid pressure waveform, with its characteristic points highlighted, (b) identification of the characteristic points from the second derivative of pressure waveform, (c) construction of multi-Rayleigh flow rate model, (d) magnitude spectrum of the impedance analysis performed in frequency domain for the estimation of characteristic impedance, (e) separation of forward and backward pressure waveforms.

## A. Identification of Fiducial Points from Second Derivative Waveform



## B. Construction of multi-Rayleigh Flow Rate Model



**Fig. 2.** Construction of multi-Rayleigh flow rate Model from parameters defined using the respective pressure waveform (a), (e) pressure waveform of a 25-year-old and 65 years old subject, with its fiducial points identified and markers, (b), (f) the second derivative waveform of the pressure waveform in (a), with its characteristic features identified, (c), (g) construction of multi-Rayleigh flow rate model based on the identified fiducial points and amplitude ratio between early systolic and late systolic peak from statistical models, (d), (h) comparison of modelled flow rate with reference flow rate waveform.

common to arterial pulse waveforms. A Rayleigh function has only a single parameter ( $\sigma$ ) to model and therefore has a computational advantage when constructing a multi-Rayleigh model. The flow rate waveform at the carotid artery up until the ejection period of the heart is modelled as a sum of multi-Rayleigh functions as in (3).

$$Q_{m-RAY}(t) = Q_{ES}(t) + Q_{LS}(t) = \sum_{i=1}^N \frac{t}{\sigma_i^2} \times e^{(-t^2/2\sigma_i^2)} \quad (3)$$

Where  $Q_{ES}(t)$  is the flow profile during the early systolic phase, and  $Q_{LS}(t)$  is the flow profile during the late systolic phase. The  $\sigma_i$  is the model input parameters, and  $N$  is the number of Rayleigh functions used to model the flow rate.

As the  $Q_{m-RAY}(t)$  is modelled without any prior information on  $Q_{REF}(t)$ , the time instant of early systolic flow peak ( $\tau_{ES\_peak}$ ), late systolic flow peak ( $\tau_{LS\_peak}$ ) and ejection period ( $\tau_{EP}$ ) of the  $Q_{REF}(t)$  are

obtained from pulse contour analysis of  $P(t)$  using second derivative waveforms (SDW) as illustrated in Fig. 2. The  $\tau_{ES\_peak}$  and  $\tau_{LS\_peak}$  are defined as the positive to negative consecutive zero-crossing after the second peak of SDW [13]. A box-whisker comparison of the respective SDW zero-crossings and reference flow peak is illustrated in the Supplementary Fig. (SF 2). The  $\tau_{EP}$  is defined as the time duration between the opening and closing of the aortic valve for each cardiac cycle. The opening of the aortic valve corresponds to the time instant of the systolic foot ( $\tau_{SF}$ ), and the closure of the aortic valve corresponds to the time instant of the dicrotic notch ( $\tau_{DN}$ ) in the  $P(t)$ .

The model parameters ( $\sigma_1$  to  $\sigma_N$  and  $N$ ) are found by iterative optimization such that the absolute error functions ( $F_1$ ,  $F_2$ ,  $F_3$  respectively) are lower than a threshold tolerance ( $\epsilon$ ) as in (4), (5), and (6) or  $N$  reaches a maximum value of 5, without converging. In the latter case, the  $N$  is selected with minimal error in the priority order of  $F_1$ ,  $F_2$  and  $F_3$ . The error threshold ( $\epsilon$ ) used in (4), (5), and (6) was kept as 0.25 % of the average heart rate of the study population ( $\sim \pm 2$  ms).

$$F_1 = |\tau_{ES\_peak}(Q_{m-RAY}(t)) - \tau_{ES\_peak}| < \epsilon \quad (4)$$

$$F_2 = |\tau_{LS\_peak}(Q_{m-RAY}(t)) - \tau_{LS\_peak}| < \epsilon \quad (5)$$

$$F_3 = |\tau_{base}(Q_{m-RAY}(t)) - \tau_{EP}| < \epsilon \quad (6)$$

Where  $\tau_{ES\_peak}$  of  $Q_{m-RAY}(t)$  is the time instant of the maximum amplitude as well as the early systole peak,  $\tau_{LS\_peak}$  of  $Q_{m-RAY}(t)$  is the time instant of late systole peak, and  $\tau_{base}$  of  $Q_{m-RAY}(t)$  is the time duration from  $t = 0$  s to the time taken to decay 99 % of the peak amplitude of  $Q_{m-RAY}(t)$  as illustrated in Fig. 2.

The separation of forward-backward pressure waveforms is independent of the actual amplitude of the flow rate [14]. Therefore, the amplitude of the  $Q_{m-RAY}(t)$  (and of the early systolic peak) after the modelling is normalized to 1, with a relative amplitude of late systolic peak in the range of 0.3 (for the younger population) to 0.6 (in the older population) obtained from a statistical model. The statistical model is an exponential regression model obtained based on the dependency of the amplitude ratio of flow peaks with  $AIx$  from the study population [27] and may be referred to in the Supplementary Fig. (SF 3). For the comparison of  $Z_C$  and for the purpose of the graphical illustration of the flow profile, the  $Q_{m-RAY}(t)$  is scaled to the actual magnitude of the peak flow rate of  $Q_{REF}(t)$ .

## 2.2. Computation

### 2.2.1. Data preparation

The dataset used for the validation of the  $WSA_{m-RAY}$  is a publicly accessible database based on Nektar1D arterial model (Pulse Wave Database) [32]. This arterial model has been clinically validated and used in several studies for simulating variations in hemodynamic parameters and generating relevant data. The database contains 4374 virtual (healthy) subjects with age ranging from 25 to 75 years. The hemodynamic variability is generated based on the age-related changes in the arterial, peripheral vascular bed, blood, and cardiac properties.

The pressure waveform (in mmHg) and flow rate waveform (ml/s) obtained from the common carotid artery were used in this study. The flow rate waveform was obtained by combining the flow velocity waveform and the carotid artery cross-sectional area waveform. Both pressure and derived flow rate waveforms were sampled at 500 Hz from the database and up-sampled to 10 kHz as part of the data processing. A total of 280 subjects who exhibited abnormal pressure ranges outside of healthy ranges were excluded from the analysis of the study. The systolic BP and diastolic BP at the carotid artery for the remaining study population varied from 81.83 mmHg to 150.80 mmHg and 50.16 mmHg to 89.89 mmHg, respectively. The peak flow rate ranged from 10.40 ml/s to 33.57 ml/s. Both  $WSA_{REF}$  and  $WSA_{m-RAY}$  were implemented using the remaining 4094 subjects.

### 2.2.2. Data processing

The second derivative of the  $P(t)$  was obtained after pre-processing with a zero-phase 2nd order Butterworth filter of cut-off frequency 75 Hz. The  $\tau_{ES\_peak}$  was computed from the time instant of positive to negative zero-crossing of the second derivative waveform (SDW) after the  $\tau_{SF}$  (the initial maxima in the SDW of  $P(t)$ ). The  $\tau_{LS\_peak}$  was computed from the next consecutive zero crossing. The  $\tau_{DN}$  was identified as a time instant of local maximum in the SDW of  $P(t)$  after the systolic peak ( $\tau_{SP}$ ). The figures illustrating the details of choice of fiducial points are included in the Supplementary Section (SF 4 and SF 5).

The model parameters of  $Q_{m-RAY}(t)$  were obtained optimally based on (4) – (6), and the peak amplitude was normalized to 1. To perform WSA for both the reference and proposed method, the  $Z_C$  was obtained from the input impedance ( $Z_0$ ) analysis ( $Z_0 = P(j\omega)/Q_{REF}(j\omega)$ ) and ( $P(j\omega)/Q_{m-RAY}(j\omega)$ ) in the frequency domain. Both the pressure waveform and the flow waveform (measured and modelled) were transformed into the frequency domain using Fast Fourier Transform (FFT). The input impedance is defined as the ratio of magnitudes of the pressure harmonics to the flow harmonics, both in the measured and modelled scenarios. The  $Z_C$  was estimated as the average magnitude of the input impedance from the 4th to 10th harmonics of  $Z_0$ . Fig. 3 depicts the implementation of  $WSA_{m-RAY}$  and  $WSA_{REF}$  for a young and older age. SF 1(c) illustrates the steps involved in the data processing of both pressure waveform and flow waveform (modelled or measured) to arrive at the forward and backward pressure waves in the Supplementary Section. All the required signal processing and analysis were developed using the LabVIEW® programming platform running on a Windows® 11 computer.

## 2.3. Statistical analysis

The error analysis between respective  $P_F(t)$  and  $P_B(t)$  from  $WSA_{REF}$  and  $WSA_{m-RAY}$  were reported as root mean square error (RMSE). The differences between  $Z_C$ ,  $\Delta P_F$ ,  $\Delta P_B$  and wave reflection quantification indices (RM, RI, RWTT) between reference and proposed methods were analyzed using two-tailed paired t-tests and reported as mean  $\pm$  standard deviation (SD) or 95 % confidence interval (CI). Equivalence testing for the abovementioned differences using a two-one-sided t-test (TOST) procedure with a  $\pm 10$  % equivalence margin was analyzed [33]. The equivalency between the reflection quantification index (RM) derived from  $WSA_{REF}$  and  $WSA_{m-RAY}$  was established with 95 % confidence if the mean difference with 90 % CI were contained within the pre-defined equivalence zone. The choice of a  $\pm 10$  % equivalence margin was based on previous research indicating that a 10 % rise in RM (reflection magnitude) corresponds to a 31 % higher risk of all-cause mortality [8]. Deviating from this equivalence range could potentially have important clinical implications in terms of risk stratification using the reflection quantification indices. A Linear regression analysis, with reflection quantification indices derived from  $WSA_{REF}$  as the independent variable and reflection quantification indices derived from  $WSA_{m-RAY}$  as a dependent variable, along with their Pearson correlation coefficient, was used to analyze the correlation and trend line between both sets of parameters. Bland-Altman analysis was constructed to analyze any progression of systematic errors and overall comparison between the two methods. A p-value of 0.05 or less was used to regard the test as statistically significant.

## 3. Results

### 3.1. Reliability of the multi-Rayleigh flow rate waveform model

The overall RMSE in the  $Q_{m-RAY}(t)$  was 3.19 ml/s. The  $Q_{m-RAY}(t)$  has captured the characteristic peaks in the flow profile of the common carotid artery with an RMSE at the time instant of the early systolic peak as 3.30 ms ( $< 0.4$  % of average heart rate) and RMSE at the time instant of late systolic peaks as 8.26 ms ( $< 1$  % of average heart rate). The RMSE

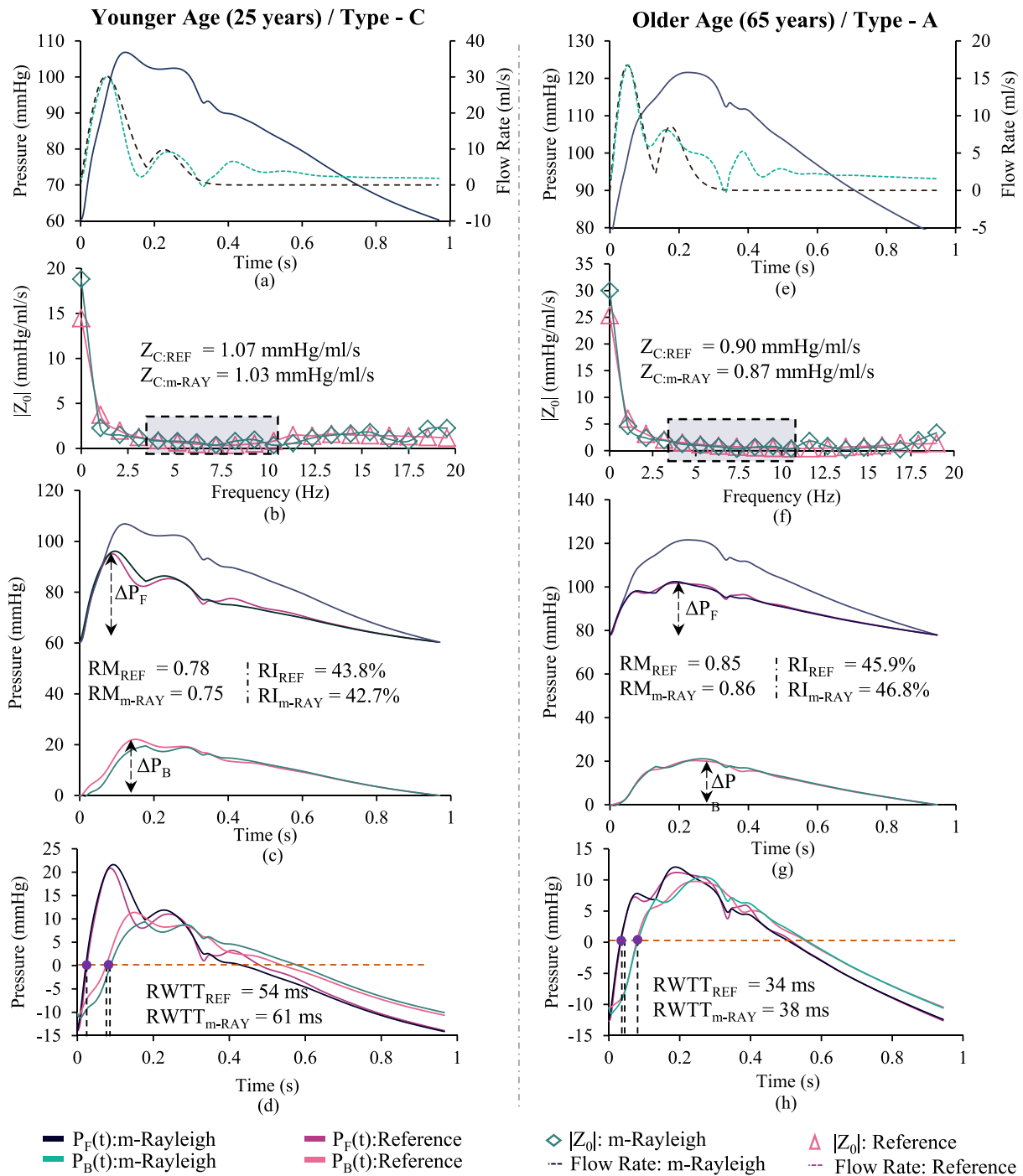


**Fig. 3.** (a), (e) Pressure waveform with reference flow and modelled flow rate waveform of a 25-year-old (Type-C, AIX: -15%) and 65-year-old (Type-A, AIX: 10%) subject, (b), (f) Input impedance spectrum obtained from pressure and flow rate waveform in frequency domain, (c), (g) Separated forward and backward waveforms and illustration of pulse pressures, (d), (h) Estimation of RWTT using the zero-crossing method.

in the time instant at the base of  $Q_{m-RAY}(t)$  was 34.31 ms (<4.5 % of average heart rate). Age-dependent changes in the flow rate waveform were reliably captured, and sample waveforms for each decade of the age group (25 years to 65 years) are illustrated in Fig. 4. The magnitude frequency spectrum of  $Q_{m-RAY}(t)$  and  $Q_{REF}(t)$  yielded a -20 dB cut-off <15 Hz and the magnitudes of harmonics exhibited substantial and statistically significant correlation ( $r \sim 0.99$ ,  $p < 0.001$ ) between both the WSA methods.

### 3.2. Agreement of $Z_C$ between $WSA_{REF}$ and $WSA_{m-RAY}$

The group average  $Z_C$  obtained from  $WSA_{m-RAY}$  was  $0.64 \pm 0.18$  mmHg/ml/s, and from  $WSA_{REF}$  was  $0.63 \pm 0.23$  mmHg/ml/s. The difference in mean values was  $0.01 \pm 0.11$  mmHg/ml/s (1.57 % change from the  $Z_{C-REF}$ ). Additionally, as depicted in Fig. 5(a), the regression analysis revealed a statistically significant and robust correlation ( $r = 0.89$ ,  $p < 0.001$ ) between both the  $Z_C$ . The Bland-Altman analysis depicted a scattered plot with no clear trend of systematic errors in Fig. 5 (b). The bias was negligible ( $-0.01 \pm 0.11$  mmHg/ml/s), with CI in the range of -0.22 mmHg/ml/s to 0.20 mmHg/ml/s.

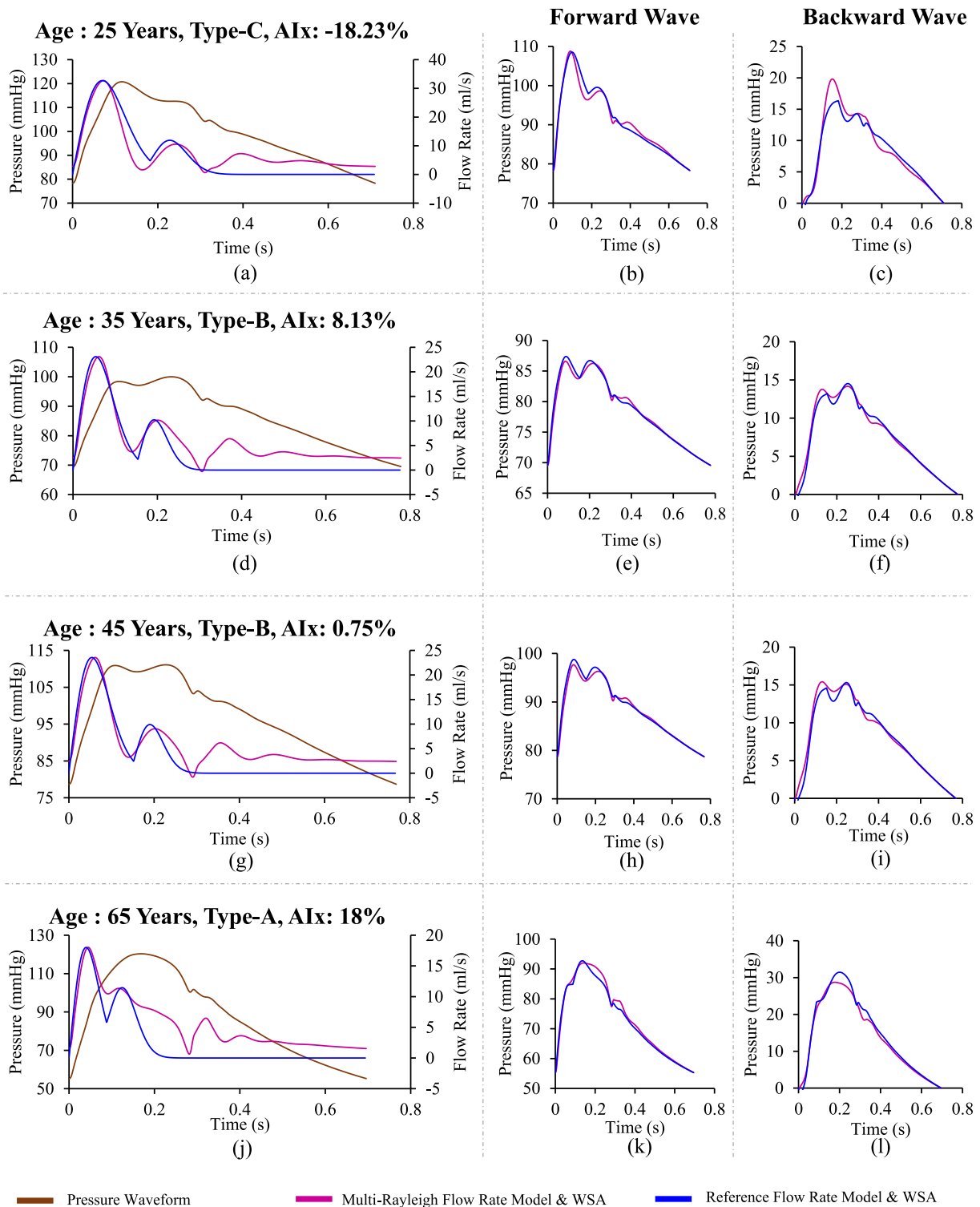


Fig. 4. Carotid WSA performed for a (a)-(c) 25-year subject, (d)-(f) 35-year subject, (g)-(i) 45-year subject, (j)-(l) 65-year subject.

### 3.3. Waveform analysis and accuracy of forward and backward waves

Fig. 4 shows the typical examples of derived  $P_F(t)$  and  $P_B(t)$  obtained from  $WSA_{REF}$  and  $WSA_{m-RAY}$  for the age group 25 years to 65 years. The group average RMSE of  $P_F(t)$  and  $P_B(t)$  derived from  $WSA_{m-RAY}$  with respect to one derived from  $WSA_{REF}$  was  $1.12 \pm 0.65$  mmHg and  $1.68 \pm 0.89$  mmHg, respectively. The group average values of  $\Delta P_F$  and  $\Delta P_B$  derived from  $WSA_{m-RAY}$  yielded  $21.29 \pm 6.54$  mmHg and  $16.84 \pm 6.52$  mmHg, respectively. The deviation in  $\Delta P_F$  was 1.18 %, and in  $\Delta P_B$  was

0.05 %, when compared between  $WSA_{REF}$  and  $WSA_{m-RAY}$ , and the difference was not statistically significant ( $p > 0.05$ ). A statistically significant and strong correlation ( $r = 0.99$ ,  $p < 0.0001$ ) between  $\Delta P_F$  derived from  $WSA_{m-RAY}$  and  $WSA_{REF}$  and between  $\Delta P_B$  derived from both methods.

### 3.4. Performance evaluation for wave reflection quantification indices

The group average value for RM, RI and RWTT derived from  $WSA_{m-}$

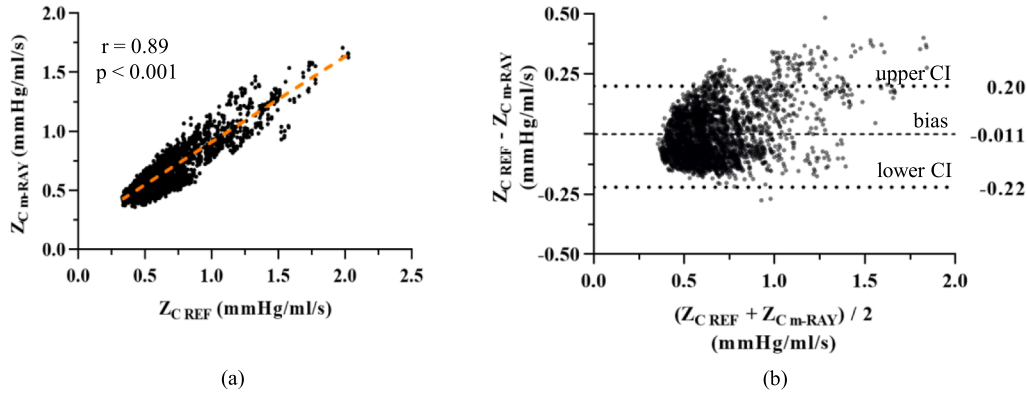


Fig. 5. (a) Regression analysis with best fit linear trend line and correlation between  $Z_{C\ REF}$  and  $Z_{C\ m-RAY}$ , (c) Bland Altman analysis between the  $Z_{C\ REF}$  and  $Z_{C\ m-RAY}$ .

RAY yielded  $0.78 \pm 0.079$ ,  $43.84 \pm 2.58\%$  and  $50.10 \pm 7.63\ ms$ , respectively, whereas for the reflection indices derived from  $WSA_{REF}$  were  $0.80 \pm 0.05$ ,  $44.47 \pm 1.86\%$  and  $45.86 \pm 9.18\ ms$  respectively. The mean differences in RM, RI and RWTT obtained from  $WSA_{REF}$ , and  $WSA_{m-RAY}$  were 0.018, 0.62% and  $-4.2\ ms$ , respectively. A 10% margin-based equivalence testing, as depicted in Fig. 6(a)-(c), revealed that the  $\Delta P_F$ ,  $\Delta P_B$  and RM derived from  $WSA_{m-RAY}$  demonstrated equivalency with the ones derived from  $WSA_{REF}$ . A strong and statistically significant correlation ( $r > 0.73$ ,  $p < 0.0001$ ) among each reflection indices from both the WSA methods was observed, as depicted in Fig. 7(a)-(c). The highest correlation was observed for RWTT ( $r = 0.83$ ,  $p < 0.0001$ ). As in Fig. 7 (d)-(f), the Bland-Altman analysis depicted a scattered plot with no clear trend of any systematic errors. The bias (CI) in reflection indices obtained from both the WSA methods were  $0.018 \pm 0.05$  (CI:  $-0.08$  to  $0.12$ ),  $0.62 \pm 1.7\%$  (CI:  $-2.8\%$  to  $4.0\%$ ), and  $-4.20 \pm 5.1\ ms$  (CI:  $-14\ ms$  to  $5.7\ ms$ ) for RM, RI and RWTT respectively.

#### 4. Discussion

In this study, we proposed a model for approximating the carotid artery flow rate waveform using multi-Rayleigh functions. The novelty of the proposed method is that no prior information on the flow waveform was necessary, and a morphologically closer physiological flow waveform was derived based on characteristic features obtained from each subject's pressure waveform morphology. The model was validated in 4374 virtual (healthy) subjects aged from 25 years to 75 years, evaluating the agreement among the  $Z_C$ ,  $P_F(t)$ ,  $P_B(t)$  and the derived reflection quantification indices (RM, RI, RWTT) between  $WSA_{m-RAY}$  and  $WSA_{REF}$ . The  $Q_{m-RAY}(t)$  captured the characteristic peaks of the carotid artery flow rate waveform in the early and late systolic phases. The relative ratio of flow peak amplitudes depends on the age-related changes in the blood vessel's structural and functional properties and

manifests in the respective pressure waveform morphology [27,34]. The relative amplitude range was obtained via an exponential regression model, analyzing the distribution of the flow peak amplitude ratio ( $A_{LS}/A_{ES}$ ) with  $AI_x$  among all the 4374 subjects as depicted in the Supplementary Fig. (SF 3). A time domain comparison of  $Q_{m-RAY}(t)$  with  $Q_{REF}(t)$  yielded lower RMSE for overall waveform morphology and for the time instants of the characteristic peaks. A frequency domain analysis revealed a strong correlation coefficient ( $r \sim 0.99$ ,  $p < 0.001$ ) between the amplitudes of the magnitude spectrum of  $Q_{m-RAY}(t)$  and  $Q_{REF}(t)$  up to a  $-20\ dB$  cut-off ( $\sim 15\ Hz$ ). The harmonics, up to  $15\ Hz$ , would generally constitute 95 – 97 percentiles of the energy content in the flow waveform [35]. The higher levels of accuracy in time domain signals and agreement in the frequency spectrum indicate that the  $Q_{REF}(t)$  was well-modelled by  $Q_{m-RAY}(t)$  for WSA. The developed  $Q_{m-RAY}(t)$  physiologically modelled the  $Q_{REF}(t)$  only up until the ejection period of the heart, as the systolic phase of the flow waveform was more significantly relevant for WSA.

The impedance analysis (IA) using the  $P(j\omega)$  with  $Q_{REF}(j\omega)$  (referred to as  $IA_{REF}$ ) and with  $Q_{m-RAY}(j\omega)$  (referred to as  $IA_{m-RAY}$ ) for the estimation of  $Z_C$  revealed bias between  $Z_{C\ m-RAY}$  and  $Z_{C\ REF}$  of negligible magnitude ( $\sim 1.73\%$ ). A previous attempt by our group to model the carotid flow waveform using multi-Gaussians [36] reported a bias between modelled and reference  $Z_C$  of 4.72%. The  $Z_C$  was estimated from the 4 to 10 harmonics of the IA. Within the 4 to 10 harmonics, a strong correlation exists ( $r \sim 0.98$ ,  $p < 0.001$ ) among the magnitude of impedance obtained from  $IA_{REF}$  and  $IA_{m-RAY}$ . The regression analysis (Fig. 5) exhibited a strong and statistically significant correlation ( $r = 0.89$ ,  $p < 0.001$ ) between  $Z_{C\ m-RAY}$  and  $Z_{C\ REF}$  and was observed to be better than our previous attempt using multi-Gaussian [36] (with an  $r = 0.78$ ,  $p < 0.001$ ). The magnitude-wise comparison of the group average values of  $Z_C$  was not possible, as the analysis in [36] was performed in arbitrary units (the peak magnitude of the multi-Gaussian flow model

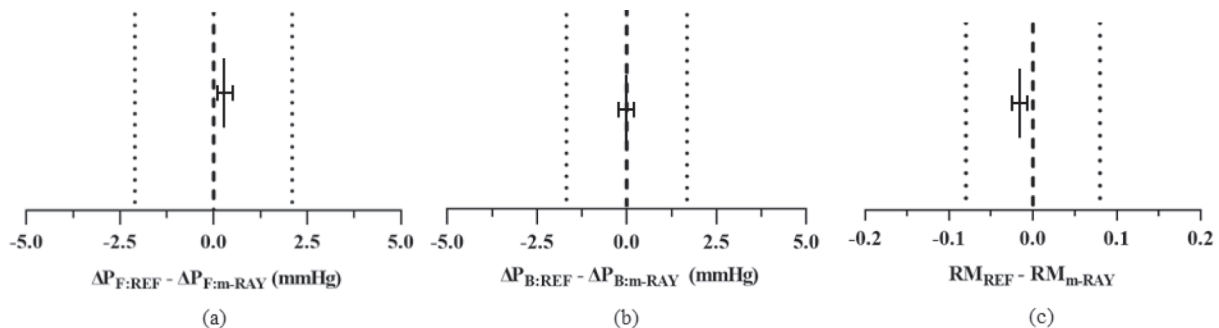


Fig. 6. Equivalence testing using TOST procedure for mean  $\pm$  95% CI for  $\Delta P_F$ ,  $\Delta P_B$  and RM.

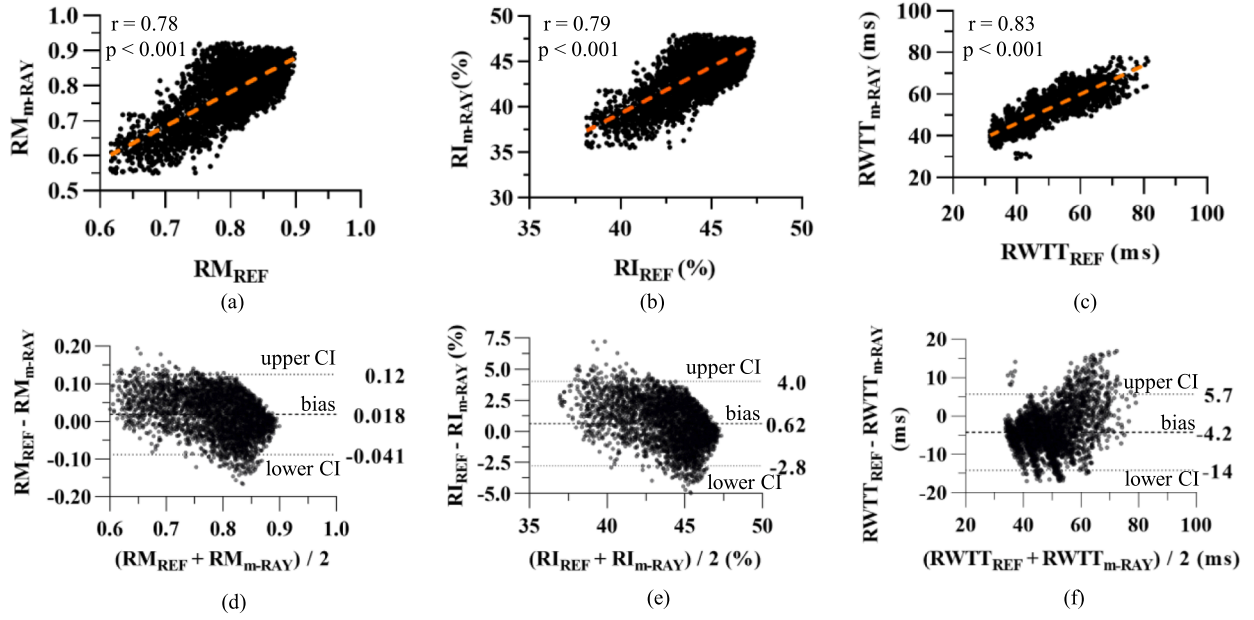


Fig. 7. (a)-(c) Regression analysis for RM, RI and RWTT obtained from  $WSA_{m-RAY}$  and  $WSA_{REF}$ , (b) Bland-Altman analysis for RM, RI and RWTT obtained from  $WSA_{m-RAY}$  and  $WSA_{REF}$ .

and reference flow was normalized to 1) and in this study as mmHg/ml/s (the peak magnitude of  $Q_{m-RAY}(t)$  was scaled to the peak value of  $Q_{REF}(t)$ ). However, it is clear from the observations that the proposed flow modelling approach using multi-Rayleigh has improved the accuracy in the estimation of  $Z_C$ , which is a vital step for the implementation of WSA.

The  $WSA_{REF}$  and  $WSA_{m-RAY}$  were successfully implemented in 4374 subjects, spanning across Type-A, Type-B and Type-C pressure waveform morphologies. The  $P_F(t)_{m-RAY}$  and  $P_B(t)_{m-RAY}$  have an RMSE less than 1.5 mmHg when compared with the respective  $P_F(t)_{REF}$  and  $P_B(t)_{REF}$ . Although not directly comparable, these accuracies (in terms of RMSE) are in the range of 0.80 to 6.66 mmHg, in line with those obtained by various aortic flow modelling approaches [14–19]. The RMSE obtained for  $P_F(t)_{m-RAY}$  and  $P_B(t)_{m-RAY}$  were similar in range with the previous attempt using multi-Gaussians-based WSA [20] for carotid flow. The deviation in  $P_F(t)_{m-RAY}$  and  $P_B(t)_{m-RAY}$  with their respective reference counterpart are statistically insignificant ( $p > 0.05$ ), suggesting the reliability of WSA performed using  $Q_{m-RAY}(t)$ . The  $P_F(t)$  and  $P_B(t)$  obtained from WSA using triangular aortic flow modelling [14] tend to generate spikes, which were absent in the  $P_F(t)$  and  $P_B(t)$  obtained using measured, lognormal [17], Windkessel-based [16], average [15] and personalized [18,19] aortic flow modelling approaches. Although the above methods were developed for modelling the Aortic flow, the conclusions drawn from comparative studies [15,18,19] suggest a physiological flow modelling is better, similar to  $Q_{m-RAY}(t)$  on which the proposed method was developed. A sample illustration of age-dependency on carotid flow modelling using  $Q_{m-RAY}(t)$  with its derived  $P_F(t)$  and  $P_B(t)$  using both  $WSA_{REF}$  and  $WSA_{m-RAY}$  is depicted in Fig. 4, highlighting the model's closeness to physiologic flow rate waveform.

The deviation in forward ( $\Delta P_F$ ) and backward ( $\Delta P_B$ ) pulse pressure obtained from  $WSA_{m-RAY}$  was within the range of 1.39 mmHg to 3.93 mmHg for  $\Delta P_F$  and 0.39 mmHg to 1.45 mmHg for  $\Delta P_B$  in studies that shared the same virtual subject's database for either aortic [19,37] or carotid flow modelling [20]. Other studies performed on *in-vivo* data [14–18] had the ranges of  $\Delta P_F$  and  $\Delta P_B$  from 0.01 to 12.18 mmHg. The bias and CI were also at par with the reported values in previous studies [14–19]. These results suggest that a more physiologic flow modelling

offers better accuracy to the  $P_F(t)$ ,  $P_B(t)$  and their amplitudes. Therefore, the results obtained here demonstrated the efficiency of the  $WSA_{m-RAY}$  in decomposing the  $P(t)$  at the carotid artery into its forward-backward components. The performance of the  $WSA_{m-RAY}$  was evaluated by comparing the magnitude quantification of reflection (RM and RI) and arrival time of reflection waves (as RWTT) with that of the  $WSA_{REF}$ .

The group average values of RM, RI and RWTT were in similar ranges as reported in the literature [14–19] for aortic flow modelling. In [15], the methodological considerations of triangular flow modelling and identification of fiducial points from the pressure waveform were independently studied in 2325 participants and reported that WSA using an average flow waveform obtained from a subset of the population (~3%) performed better than the WSA based on triangular flow approximation. In [16], WSA based on Windkessel modelling of aortic flow reported similar performance to WSA using average flow and better than that using triangular flow approximation. The excess pressure waveform, obtained from the reservoir-wave model has morphological similarities to the flow waveform, and has been proposed for modelling peripheral flow [21]; However, the studies were limited to aortic WSA [38–40]. Recently lognormal approximation of aortic flow [17] was suggested as an alternative to triangle flow. However, the validation was examined in smaller cohorts (~11 participants), and the determination of the model parameter was not well described. The lognormal WSA was evaluated in a virtual subject's database (~4374 participants) and with invasively acquired data (~13 participants) [19] to compare the performance against the triangular, measured and personalized aortic flow model. The personalized flow waveform was more consistent with the measured flow waveform, yielding better agreement in RM, RI and RWTT with reference WSA.

The group average values for RM, RI and RWTT were in the range of those obtained using multi-gaussian WSA for the carotid artery [20]. TABLE 1 highlights the group average values obtained from WSA using multi-Rayleigh and multi-Gaussian models. TABLE 2 summarizes the correlation of reflection quantification indices obtained from each method with the ones obtained from  $WSA_{REF}$ . The method described in [20] depends on an empirical relationship derived from the multi-Gaussian decomposition of  $P(t)$ . The  $P_F(t)$  and  $P_B(t)$  were derived by uniquely combing a set of multi-Gaussians based on a pre-determined

**Table 1**

Comparison of reflection quantification indices between  $WSA_{REF}$ ,  $WSA_{m-RAY}$  and  $WSA_{MG}$ .

Reflection Quantification Indices	Group Average		
	$WSA_{REF}$	$WSA_{m-RAY}$	$WSA_{MG}$
Forward Pulse Pressure, $\Delta P_F$ (mmHg)	22.25 ± 5.86	21.29 ± 6.54	23.05 ± 7.04
Backward Pulse Pressure, $\Delta P_B$ (mmHg)	16.04 ± 5.45	16.84 ± 6.52	17.75 ± 5.92
Reflection Magnitude, RM	0.80 ± 0.05	0.78 ± 0.079	0.79 ± 0.08
Reflection Index, RI (%)	44.47 ± 1.86	43.84 ± 2.58	44.23 ± 2.58
Reflection Wave Transit Time, RWTT (ms)	45.86 ± 9.18	50.10 ± 7.63	45.50 ± 5.56

**Table 2**

Correlation with reflection quantification indices of  $WSA_{m-RAY}$  and  $WSA_{MG}$  with  $WSA_{REF}$ .

Reflection Quantification Indices	Correlation with $WSA_{REF}$	
	$WSA_{m-RAY}$	$WSA_{MG}$
Forward Pulse Pressure, $\Delta P_F$ (mmHg)	$r = 0.99$	$r = 0.96$
Backward Pulse Pressure, $\Delta P_B$ (mmHg)	$r = 0.99$	$r = 0.97$
Reflection Magnitude, RM	$r = 0.78$	$r = 0.82$
Reflection Index, RI (%)	$r = 0.79$	$r = 0.83$
Reflection Wave Transit Time, RWTT (ms)	$r = 0.84$	$r = 0.76$

look-up table for optimized model parameters for each type of pressure waveform morphology. This required a training set (~20 % of the population) with reference flow waveform to determine the optimized design parameters. The approach was similar to the method described in [15], which uses a subset of the study population (~3%) to obtain an average flow waveform. The higher values of correlation for RM and RI in [20] were associated with the closeness of the model to the study population, as observed in both [15,20]. However, more physiologic flow modelling using  $WSA_{m-RAY}$  proved to be effective in quantifying RWTT better than using multi-Gaussian model. The proposed method is also computationally less demanding, at least three orders less than the multi-Gaussian based WSA model.

Aortic WSA, when implemented using non-invasive measurement techniques, relies on calibrated or scaled aortic pressure waveform obtained either from radial or carotid tonometry waveform via generalized transfer functions [13] and the aortic flow measured using doppler echocardiography or MRI. In certain studies, the carotid tonometry waveforms were scaled to the carotid pressure waveforms via calibration and used alongside LVOT flow waveforms for WSA [15], as the carotid artery closely resembles the central blood pressure and aortic conditions. As such, the WSA can be implemented at any arterial site where both pressure and flow measurements are available. For instance, modelled or measured carotid artery flow rate waveform along with measurement of pressure waveform from the same arterial site has been reported to have clinical significance on cerebral-vascular pathophysiology. The mainstream of cerebral blood flow occurs via both the left and right common carotid arteries and the separated forward-backward pressure and flow waveforms was used to perform the wave intensity analysis, which reported a significant association between wave reflection quantification and the rate of cognitive decline [22]. The carotid arteries have the anatomical advantage of being superficial and increase the ease of non-invasive measurements. The carotid artery is a surrogate of central [41] and cerebral haemodynamics [42]. This opened up research possibilities to study the pulse dynamics of carotid arteries under physiologic perturbations induced by exercise [29,30], lower body negative/positive pressure [43], cold pressor test for carotid reactivity [44], change in distensibility [45], intensity analysis [25,46] using pressure and flow waveforms. To the best of our knowledge, the

carotid WSA was limited to [22,25,29,30,39,46,47], which measures both flow velocity or flow rate with a scaled or calibrated form of carotid pressure waveform. The method proposed in this article has demonstrated the ability to model the carotid flow rate waveform for performing WSA. The technique would potentially widen the scope of carotid WSA, its scalability and applicability to conduct more extensive cohort studies, especially on cerebral and central haemodynamics.

## 5. Limitations and future scope

The developed carotid flow rate model using multi-Rayleigh functions has demonstrated its ability to capture the characteristic features of the carotid flow rate waveform in healthy participants using an extensively validated database of simulated waveforms. An in-vivo validation study comprising the healthy and diseased population is warranted to substantiate the results obtained using the simulated virtual subject's database. The model depends on the accurate identification of fiducial points on the pressure waveform, which requires signal acquisition systems of higher sampling rates (~250 Hz and above) to identify and characterize the fiducial points accurately. Determining the relative amplitudes between the early and late systolic peaks for the carotid artery flow rate waveform was implemented as a statistical model based on its dependency on age and AIx. From the modelling perspective, works are in progress to better predict the amplitude ratio of peak flow rate with probabilistic and learning-based algorithms. It is also important to model the retrograde flow, which is not prominent in healthy participants but a significant characteristic for the diseased or aged population. Modelling of retrograde flow becomes essential when applying the concepts of WSA to peripheral arterial sites. Clinical and epidemiological trials are a need to investigate the clinical significance of reflection quantification indices (RM, RI and RWTT) as a prognostic marker of cardiovascular health, morbidity, and mortality.

## 6. Conclusion

A physiologic and personalized model for carotid artery flow rate waveform was developed using the multi-Rayleigh function for separating forward and backward waves using WSA. The modelled flow rate waveform was compared with the reference flow rate waveform, and the performance of WSA was evaluated by comparing the agreement on reflection quantification indices such as RM, RI and RWTT. The validation study to prove the feasibility of the proposed method was conducted on a simulated database of 4375 healthy participants over the age group of 25 years to 75 years. The  $P_F(t)$  and  $P_B(t)$  obtained from  $WSA_{m-RAY}$  were morphologically similar to the ones obtained from  $WSA_{REF}$ , with an RMSE < 1.5 mmHg. A strong and statistically significant correlation ( $r > 0.78$ ,  $p < 0.001$ ) was observed for all the reflection quantification indices between  $WSA_{m-RAY}$  and  $WSA_{REF}$ . The utilization of these methods in carotid artery WSA has the potential to broaden the range of vascular screenings and diagnostics that depend on the dynamics of single pulse waveforms.

## CRedit authorship contribution statement

**Rahul Manoj:** Conceptualization, Data curation, Formal analysis, Investigation, Methodology, Software, Validation, Visualization, Writing – original draft. **P.M. Nabeel:** Funding acquisition, Investigation, Project administration, Resources, Supervision, Visualization, Writing – review & editing. **V. Raj Kiran:** Conceptualization, Methodology, Project administration, Resources, Software, Supervision, Writing – review & editing. **Mohanasankar Sivaprakasam:** Funding acquisition, Project administration, Supervision, Writing – review & editing. **Jayaraj Joseph:** Funding acquisition, Investigation, Methodology, Project administration, Resources, Supervision, Writing – review & editing.

## Declaration of competing interest

The authors declare that they have no known competing financial interests or personal relationships that could have appeared to influence the work reported in this paper.

## Data availability

Data will be made available on request.

## Appendix A. Supplementary data

Supplementary data to this article can be found online at <https://doi.org/10.1016/j.bspc.2024.106129>.

## References

- J.P. Mynard, A. Kondiboyina, Wave reflection in the arterial tree, in: J.A. Chirinos (Ed.), *Textb. Arter. Stiffness Pulsatile Hemodynamics Heal. Dis.*, Academic Press, 2022: pp. 169–194. [10.1016/B978-0-323-91391-1.00011-X](https://doi.org/10.1016/B978-0-323-91391-1.00011-X).
- T. Weber, S. Wassertheurer, M. Rammer, A. Haiden, B. Hametner, B. Eber, Wave reflections, assessed with a novel method for pulse wave separation, are associated with end-organ damage and clinical outcomes, *Hypertension* 60 (2012) 534–541, <https://doi.org/10.1161/HYPERTENSIONAHA.112.194571>.
- A.W. Haider, M.G. Larson, S.S. Franklin, D. Levy, Systolic blood pressure, diastolic blood pressure, and pulse pressure as predictors of risk for congestive heart failure in the Framingham heart study background: although hypertension is a principal precursor of, *Ann. Intern. Med.* 138 (2013) 10–16, <https://doi.org/10.7326/0003-4819-138-1-200301070-00006>.
- R. Zannoli, P. Schiereck, F. Celletti, A. Branzi, B. Magnani, Effects of wave reflection timing on left ventricular mechanics, *J. Biomech.* 32 (1999) 249–254, [https://doi.org/10.1016/S0021-9290\(98\)00144-4](https://doi.org/10.1016/S0021-9290(98)00144-4).
- P. Zamani, D.A. Bluemke, D.R. Jacobs, D.A. Duprez, R. Kronmal, S.M. Lilly, V. A. Ferrari, R.R. Townsend, J.A. Lima, M. Budoff, P. Segers, P. Hannan, J. A. Chirinos, Resistive and pulsatile arterial load as predictors of left ventricular mass and geometry the multi-ethnic study of atherosclerosis, *Hypertension* 65 (1) (2015) 85–92.
- J.A. Chirinos, J.G. Kips, D.R. Jacobs, L. Brumback, D.A. Duprez, R. Kronmal, D. A. Bluemke, R.R. Townsend, S. Vermeersch, P. Segers, Arterial wave reflections and incident cardiovascular events and heart failure: MESA (multiethnic study of atherosclerosis), *J. Am. Coll. Cardiol.* 60 (21) (2012) 2170–2177.
- P. Zamani, D.R. Jacobs, P. Segers, D.A. Duprez, L. Brumback, R.A. Kronmal, S. M. Lilly, R.R. Townsend, M. Budoff, J.A. Lima, P. Hannan, J.A. Chirinos, Reflection magnitude as a predictor of mortality the multi-ethnic study of atherosclerosis, *Hypertension* 64 (5) (2014) 958–964.
- J.A. Chirinos, Deep phenotyping of systemic arterial hemodynamics in HFpEF (Part 2): Clinical and therapeutic considerations, *J. Cardiovasc. Transl. Res.* 10 (2017) 261–274, <https://doi.org/10.1007/s12265-017-9736-2>.
- P. Segers, E.R. Rietzschel, M.L. De Buyzere, D. De Bacquer, L.M. Van Bortel, G. De Backer, T.C. Gillebert, P.R. Verdonck, Assessment of pressure wave reflection: getting the timing right!, *Physiol. Meas.* 28 (2007) 1045–1056, <https://doi.org/10.1088/0967-3334/28/9/006>.
- A.D. Hughes, C. Park, J. Davies, D. Francis, S.A. McG Thom, J. Mayet, K.H. Parker, Limitations of augmentation index in the assessment of wave reflection in normotensive healthy individuals, *PLoS ONE* 8 (2013) 1–8, <https://doi.org/10.1371/journal.pone.0059371>.
- N. Westerhof, P. Sipkema, G.C.V. Den Bos, G. Elzinga, Forward and backward waves in the arterial system, *Cardiovasc. Res.* 6 (1972) 648–656, <https://doi.org/10.1093/cvr/6.6.648>.
- K.H. Parker, An introduction to wave intensity analysis, *Med. Biol. Eng. Comput.* 47 (2009) 175–188, <https://doi.org/10.1007/s11517-009-0439-y>.
- A. Qasem, A. Avolio, Determination of aortic pulse wave velocity from waveform decomposition of the central aortic pressure pulse, *Hypertension* 51 (2008) 188–195, <https://doi.org/10.1161/HYPERTENSIONAHA.107.092676>.
- B.E. Westerhof, I. Guelen, N. Westerhof, J.M. Karemaker, A. Avolio, Quantification of wave reflection in the human aorta from pressure alone: A proof of principle, *Hypertension* 48 (2006) 595–601, <https://doi.org/10.1161/01.HYP.0000238330.08894.17>.
- J.G. Kips, E.R. Rietzschel, M.L. De Buyzere, B.E. Westerhof, T.C. Gillebert, L.M. Van Bortel, P. Segers, Evaluation of noninvasive methods to assess wave reflection and pulse transit time from the pressure waveform alone, *Hypertension* 53 (2009) 142–149, <https://doi.org/10.1161/HYPERTENSIONAHA.108.123109>.
- B. Hametner, S. Wassertheurer, J. Kropf, C. Mayer, A. Holzinger, B. Eber, T. Weber, Wave reflection quantification based on pressure waveforms alone—methods, comparison, and clinical covariates, *Comput. Methods Programs Biomed.* 109 (2013) 250–259, <https://doi.org/10.1016/j.cmpb.2012.10.005>.
- L. Hao, Q. Zhang, X. Chen, Y. Yao, L. Xu, Feasibility of waveform separation of central aortic pressure pulse based on lognormal flow wave approximation, *Biomed. Signal Process. Control.* 77 (2022) 103784, <https://doi.org/10.1016/j.bspc.2022.103784>.
- N. Shenouda, J.M. Stock, J.C. Patik, J.A. Chirinos, D.G. Edwards, Personalized physiologic flow waveforms improve wave reflection estimates compared to triangular flow waveforms in adults, *Am. J. Physiol. - Hear. Circ. Physiol.* 320 (2021) H1802–H1812. [10.1152/ajpheart.00747.2020](https://doi.org/10.1152/ajpheart.00747.2020).
- H. Sun, Y. Yao, W. Liu, S. Zhou, S. Du, J. Tan, Y. Yu, L. Xu, A. Avolio, Wave reflection quantification analysis and personalized flow wave estimation based on the central aortic pressure waveform, *Front. Physiol.* 14 (2023) 1–17, <https://doi.org/10.3389/fphys.2023.1097879>.
- R. Manoj, K.V. Raj, P.M. Nabeel, M. Sivaprakasam, J. Joseph, Arterial pressure pulse wave separation analysis using a multi-Gaussian decomposition model, *Physiol. Meas.* 43 (2022) 055005, <https://doi.org/10.1088/1361-6579/ac6e56>.
- M.K. Armstrong, M.G. Schultz, A.D. Hughes, D.S. Picone, J.A. Black, N. Dwyer, P. Roberts-Thomson, J.E. Sharman, Excess pressure as an analogue of blood flow velocity, *J. Hypertens.* 39 (2021) 421–427, <https://doi.org/10.1097/HJH.0000000000002662>.
- S.T. Chiesa, S. Masi, M.J. Shipley, E.A. Ellins, A.G. Fraser, A.D. Hughes, R.S. Patel, A.W. Khir, J.P. Halcox, A. Singh-Manoux, M. Kivimaki, D.S. Celermajer, J.E. Deanfield, Carotid artery wave intensity in mid-to late-life predicts cognitive decline: The Whitehall II study, *Eur. Heart J.* 40 (2019) 2300–2309. [10.1093/eurheartj/ehz189](https://doi.org/10.1093/eurheartj/ehz189).
- E.C. Schroeder, W.K. Lefferts, T.I.M. Hilgenkamp, B. Fernhall, Acute systemic inflammation reduces both carotid and aortic wave reflection in healthy adults, *Physiol. Rep.* 7 (2019). [10.14814/phy2.14203](https://doi.org/10.14814/phy2.14203).
- W.K. Lefferts, J.A. Augustine, K.S. Heffernan, Effect of acute resistance exercise on carotid artery stiffness and cerebral blood flow pulsatility, *Front. Physiol.* 5 MAR (2014) 1–10. [10.3389/fphys.2014.00101](https://doi.org/10.3389/fphys.2014.00101).
- N. Ohte, H. Narita, M. Sugawara, K. Niki, T. Okada, A. Harada, J. Hayano, G. Kimura, Clinical usefulness of carotid arterial wave intensity in assessing left ventricular systolic and early diastolic performance, *Heart Vessels.* 18 (2003) 107–111, <https://doi.org/10.1007/s00380-003-0700-5>.
- K. Hirata, T. Yaginuma, M.F. O'Rourke, M. Kawakami, Age-related changes in carotid artery flow and pressure pulses: Possible implications for cerebral microvascular disease, *Stroke.* 37 (2006) 2552–2556, <https://doi.org/10.1161/01.STR.0000242289.20381.f4>.
- J. Hashimoto, B.E. Westerhof, S. Ito, Carotid flow augmentation, arterial aging, and cerebral white matter hyperintensities: Comparison with pressure augmentation, *Arterioscler. Thromb. Vasc. Biol.* 38 (2018) 2843–2853, <https://doi.org/10.1161/ATVBAHA.118.311873>.
- G.A. Bateman, Pulse wave encephalopathy: a spectrum hypothesis incorporating Alzheimer's disease, vascular dementia and normal pressure hydrocephalus, *Med. Hypotheses.* 62 (2004) 182–187, [https://doi.org/10.1016/S0306-9877\(03\)00330-X](https://doi.org/10.1016/S0306-9877(03)00330-X).
- N. Pomella, E.N. Wilhelm, C. Kolyva, J. González-Alonso, M. Rakobowchuk, A.W. Khir, Common carotid artery diameter, blood flow velocity and wave intensity responses at rest and during exercise in young healthy humans: A reproducibility study, *Ultrasound Med. Biol.* 43 (2017) 943–957. [10.1016/j.ultrasmedbio.2016.12.018](https://doi.org/10.1016/j.ultrasmedbio.2016.12.018).
- N. Pomella, E.N. Wilhelm, C. Kolyva, J. González-Alonso, M. Rakobowchuk, A.W. Khir, Noninvasive assessment of the common carotid artery hemodynamics with increasing exercise work rate using wave intensity analysis, *Am. J. Physiol. - Hear. Circ. Physiol.* 315 (2018) H233–H241. [10.1152/ajpheart.00667.2017](https://doi.org/10.1152/ajpheart.00667.2017).
- M. Masuda, T. Emoto, A. Suzuki, M. Akutagawa, T. Kitawaki, K. Kitaoka, H. Tanaka, S. Obara, K. Yoshizaki, S. Konaka, Y. Kinouchi, Evaluation of blood flow velocity waveform in common carotid artery using multi-branched arterial segment model of human arteries, *biomed. Signal process. Control.* 8 (2013) 509–519, <https://doi.org/10.1016/j.bspc.2013.05.005>.
- P.H. Charlton, J.M. Harana, S. Vennin, Y. Li, P. Chowieniczky, J. Alastruey, Modeling arterial pulse waves in healthy aging: a database for in silico evaluation of hemodynamics and pulse wave indexes, *Am. J. Physiol. - Hear. Circ. Physiol.* 317 (2019) H1062–H1085. [10.1152/AJPHEART.00218.2019](https://doi.org/10.1152/AJPHEART.00218.2019).
- E. Walker, A.S. Nowacki, Understanding equivalence and noninferiority testing, *J. Gen. Intern. Med.* 26 (2011) 192–196. [10.1007/s11606-010-1513-8](https://doi.org/10.1007/s11606-010-1513-8).
- K.S. Heffernan, W.K. Lefferts, J.A. Augustine, Hemodynamic correlates of late systolic flow velocity augmentation in the carotid artery, *Int. J. Hypertens.* 2013 (2013), <https://doi.org/10.1155/2013/920605>.
- D.W. Holdsworth, C.J.D. Norley, R. Frayne, D.A. Steinman, B.K. Rutt, Characterization of common carotid artery blood-flow waveforms in normal human subjects, *Physiol. Meas.* 20 (1999) 219–240, <https://doi.org/10.1088/0967-3334/20/3/301>.
- R. Manoj, V. Raj Kiran, P.M. Nabeel, M. Sivaprakasam, J. Joseph, Estimation of characteristic impedance using multi-gaussian modelled flow velocity waveform: A virtual subjects study, in: *Proc. Annu. Int. Conf. IEEE Eng. Med. Biol. Soc. EMBS, Institute of Electrical and Electronics Engineers Inc.*, 2022: pp. 2274–2277. [10.1109/EMBC48229.2022.9871684](https://doi.org/10.1109/EMBC48229.2022.9871684).
- B. Hametner, M. Schneider, S. Parragh, S. Wassertheurer, Computational assessment of model-based wave separation using a database of virtual subjects, *J. Biomech.* 64 (2017) 26–31, <https://doi.org/10.1016/j.jbiomech.2017.08.027>.
- M.K. Armstrong, J.A. Chirinos, G.K. Kapuku, G.L. Pierce, Aortic pressure-only wave separation analysis in adolescents: accuracy and associations with left ventricular mass index, *J. Hum. Hypertens.* (2022) 1–8, <https://doi.org/10.1038/s41371-022-00757-y>.
- N. Di Lascio, V. Gemignani, E. Bianchini, R.M. Bruno, L. Ghiadoni, F. Faia, Effects of carotid pressure waveforms on the results of wave separation, wave intensity and reservoir pressure analysis, *Physiol. Meas.* 39 (2018), <https://doi.org/10.1088/1361-6579/aae6eb>.

- [40] M. Michail, O. Narayan, K.H. Parker, J.D. Cameron, Relationship of aortic excess pressure obtained using pressure-only reservoir pressure analysis to directly measured aortic flow in humans, *Physiol. Meas.* 39 (2018), <https://doi.org/10.1088/1361-6579/aaca87>.
- [41] D. Terentes-Printzios, V. Gardikioti, C. Vlachopoulos, Central over peripheral blood pressure: an emerging issue in hypertension research, *Hear. Lung Circ.* 30 (2021) 1667–1674, <https://doi.org/10.1016/j.hlc.2021.07.019>.
- [42] C.E. Raphael, M. Frenneaux, Wave intensity and cognitive decline: where the heart leads the mind follows, *Eur. Heart J.* 40 (2019) 2310–2312, <https://doi.org/10.1093/eurheartj/ehz307>.
- [43] K.V. Raj, P.M. Nabeel, D. Chandran, M. Sivaprakasam, J. Joseph, High-frame-rate A-mode ultrasound for calibration-free cuffless carotid pressure: feasibility study using lower body negative pressure intervention, *Blood Press.* 31 (2022) 19–30, <https://doi.org/10.1080/08037051.2021.2022453>.
- [44] A.C.C.M. Van Mil, Y. Hartman, F. Van Oorschot, A. Heemels, N. Bax, E.A. Dawson, N. Hopkins, M.T.E. Hopman, D.J. Green, D.L. Oxborough, D.H.J. Thijssen, Correlation of carotid artery reactivity with cardiovascular risk factors and coronary artery vasodilator responses in asymptomatic, healthy volunteers, *J. Hypertens.* 35 (2017) 1026–1034, <https://doi.org/10.1097/HJH.0000000000001274>.
- [45] P.M. Nabeel, K.V. Raj, J. Joseph, Image-free ultrasound for local and regional vascular stiffness assessment: The ARTSENS Plus, *J. Hypertens.* 40 (2022) 1537–1544, <https://doi.org/10.1097/HJH.0000000000003181>.
- [46] K. Niki, M. Sugawara, D. Chang, A. Harada, T. Okada, R. Sakai, K. Uchida, R. Tanaka, C.E. Mumford, A new noninvasive measurement system for wave intensity: Evaluation of carotid arterial wave intensity and reproducibility, *Heart Vessels.* 17 (2002) 12–21, <https://doi.org/10.1007/s003800200037>.
- [47] A. Zambanini, S.L. Cunningham, K.H. Parker, A.W. Khir, S.A.M.G. Thom, A. D. Hughes, Wave-energy patterns in carotid, brachial, and radial arteries: A noninvasive approach using wave-intensity analysis, *Am. J. Physiol. - Hear. Circ. Physiol.* 289 (2005) 270–276, <https://doi.org/10.1152/ajpheart.00636.2003>.